Bayesian Structure-Preserving Image Contrast Enhancement and Its Simplification

Tzu-Cheng Jen and Sheng-Jyh Wang, *Member, IEEE*

***Abstract*—In this paper, an efficient Bayesian framework is proposed for image contrast enhancement. Based on the image acquisition pipeline, we model the image enhancement problem as a maximum *a posteriori* (MAP) estimation problem, where the posteriori probability is formulated based on the local information of the given image. In our framework, we express the likelihood model as a local image structure preserving constraint, where the overall effect of the shutter speed and camera response function is approximated as a linear transformation. On the other hand, we design the prior model based on the observed image and some statistical property of natural images. With the proposed framework, we can effectively enhance the contrast of the image in a natural-looking way, while with fewer artifacts at the same time. Moreover, in order to apply the proposed MAP formulation to typical enhancement problems, like image editing, we further convert the estimation process into an intensity mapping process, which can achieve comparable enhancement performance with a much lower computational complexity. Simulation results have demonstrated the feasibility of the proposed framework in providing flexible and effective contrast enhancement.**

***Index Terms*—Contrast enhancement, maximum *a posteriori* (MAP) estimation.**

I. Introduction

CAPTURING images under poor illumination or inappropriate camera settings may generate images of inadequate contrast. Up to now, plentiful algorithms have been proposed to improve the visual quality of poorly illuminated images [1]–[29]. Among these algorithms, histogram equalization (HE) [1] has been widely used and has been thought of as the ancestor of many histogram-based contrast enhancement algorithms. The principle of the HE algorithm is to use the cumulative distribution function as an intensity mapping function to extend the effective dynamic range of the original image. Even though the HE algorithm is adaptive and efficient in image enhancement, it may generate undesired defects, like overly enhanced results, noise amplification, and loss of fine details.

After HE, plentiful variants have been proposed for contrast enhancement. For example, [2]–[7] aimed for mean-preserving histogram equalization. In [2], the author divided the original histogram into two subhistograms and applied the equalization process over each subhistogram for mean-preserving. In [3] and [4], the original histogram is divided in a similar way based on a theoretical threshold value, rather than the intensity mean used in [2]. In [5]–[7], the original histogram is further divided into multiple subhistograms based on certain criteria for mean-preserving equalization. In [5], the separation procedure defined in [2] is applied to each subhistogram recursively. In [6], the original histogram is divided into multiple histogram based the location of local maxima in the histogram. Basically, these mean-preserving HE algorithms can effectively suppress the over-enhancement problem, but may sometimes restrain the degree of contrast enhancement due to the inclusion of the mean-preserving constraint.

On the other hand, the authors in [8]–[13] claimed that the over-enhancement problem in histogram equalization is usually due to some extremely high peaks in the histogram. In their approaches, the shape of the histogram is modified before the equalization process. In [8], a simple clipping operation is applied for the adjustment of histogram shape. In [9], the histogram shape is modified by using a nonlinear transformation function. In [10], the authors formulated the histogram modification problem as an optimization problem and some prior information about the histogram shape is included. In [11], the author modified the cumulative distribution function for the control of the enhancement level. In [12] and [13], the authors formed histogram bins and optimally redistributed the bins within the available dynamic range. Even through these shape modification methods may also effectively deal with the over-enhancement problem, they neglect the local image information that could be very helpful for contrast enhancement.

To include local information, a few histogram-based approaches look for adaptive histogram equalization (AHE), which relies on localized image data [14], [15]. Although these AHE methods can better enhance fine details, they usually suffer from the over-enhancement problem and may amplify the blocking artifacts for compressed images.

Besides histogram-based methods, retinex-based algorithms are also popular for contrast enhancement. Retinex-based approaches aim to remove from an image the influence of the luminance component. In [16] and [17], the authors estimated the reflectance component of a given image by calculating the ratio between the original image data and its low-pass filtered version. The estimated reflectance component is then adjusted by a nonlinear transformation to achieve contrast

Manuscript received February 16, 2011; revised July 7, 2011 and September 16, 2011; accepted September 26, 2011. Date of publication November 23, 2011; date of current version May 31, 2012. This work was supported by the National Science Council of Taiwan, under Grant NSC-98-2221-E-009-110-MY3. This paper was recommended by Associate Editor W.-J. Zeng.

The authors are with the Department of Electronics Engineering, Institute of Electronic, National Chiao Tung University, Hsinchu 300, Taiwan (e-mail: eejen.ee91g@g2.nctu.edu.tw; shengjyh@faculty.nctu.edu.tw).

Color versions of one or more of the figures in this paper are available online at http://ieeexplore.ieee.org.

Digital Object Identifier 10.1109/TCSVT.2011.2177184

enhancement. Unlike [16] and [17], the approaches in [18] and [19] modify the luminance component. In [18], the estimated luminance component is modified by a gamma function. In [19], the authors proposed a two-stage scheme, which first applies a windowed inverse sigmoid function for dynamic range compression, and then applies a gamma function for mid-tone frequency enhancement. These retinex-based approaches usually offer impressive enhancement results. However, halo effects may appear around strong edges due to the imperfect estimation of the luminance component. Besides, noise component in dark areas may also get dramatically amplified.

Unlike the above methods, some other algorithms focus on frequency-domain processing. Due to its compatibility to existing image compression standards, processing in the DCT domain has attracted great attention. The strategy of most DCT-domain approaches is to scale the DC and AC coefficients adaptively. For example, in [20], the scaling factors are related to the root of the magnitude of DCT coefficients. In [21], the authors first defined a contrast measure in the compressed domain. The contrast measure between successive bands of AC coefficients is then scaled for enhancement. Lee [22] proposed a similar approach for AC coefficients adjustment, but in an adaptive way for every image block. In [23], a parametric intensity transfer function is adopted to adjust the DC coefficient. After that, an adaptive scaling mechanism is applied to the processed image for local contrast preservation. Even though these DCT domain-based approaches may effectively enhance image contrast, they usually suffer from undesired blocking artifacts, which may seriously degrade the visual quality of the processed image.

On the other hand, some approaches treat contrast enhancement as an optimization problem [24]–[28]. The main advantage of these optimization-based approaches is their flexibility in including various kinds of desired properties for the enhanced images. For example, in [24] and [25], the authors aimed to find an optimal intensity mapping function for image enhancement so that the entropy of the processed image reaches its maximum while the deviation of the mean intensity value reaches its minimum. In [26], the authors focused on finding a mapping function that produces an image realization with maximal signal variation. In [28], for each image region, the authors found a local optimal linear transformation to retain the local image structure during the enhancement process. In their algorithm, the finding of the scaling and offset parameters of the linear transformation is formulated as an optimization problem, with the inclusion of some prior information about the scaling parameter. Although these optimization-based approaches can effectively enhance the visual quality of the processed image, their computational complexity is usually high for typical applications.

Even though these aforementioned approaches deal with the image enhancement problem from various aspects, most of them do not take into account the image acquisition process, which directly influence the visual quality of the captured images. Besides, most contrast enhancement algorithms do not consider the statistical properties of natural images. In this paper, we propose a Bayesian framework to take into account both issues. In our framework, we design the likelihood model of the Bayesian framework based on a few factors that may influence the quality of the captured images, like shutter speed and camera response function (CRF). With proper simplification, we express the overall effect of shutter speed and CRF as a local image structure preserving constraint. On the other hand, we design the prior model based on the observed image and some statistical property of natural images. With the proposed likelihood model and prior model, our framework can effectively enhance the contrast of the image in a natural-looking way, while properly suppressing undesirable artifacts and noise at the same time. Moreover, since the proposed Bayesian framework is a high dimensional optimization process, which is very time-consuming, we further propose a simplified Bayesian framework that can achieve comparable performance but with much lower computation complexity. In this paper, we first present the concept of the proposed Bayesian framework in Section II. A few simulation results are demonstrated to verify the feasibility of the proposed framework. In Section III, we further present the simplified Bayesian framework, together with some simulation results. Finally, in Section IV, conclusions are drawn.

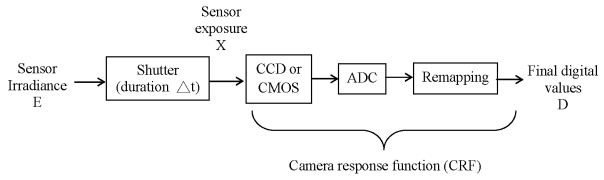

Fig. 1. Flow of image acquisition process.

II. Proposed Bayesian Framework

A. Image Acquisition Pipeline

Since the design of our framework is partially based on the image acquisition pipeline, we first review the imaging process. As illustrated in Fig. 1, we show a simplified process flow of the imaging pipeline based on the model in [30]. The camera shutter controls how long the CCD or CMOS sensor is exposed to the irradiance E. If the exposure period is Δt and the sensor irradiance at a pixel is E, the total energy X recorded at that pixel is

$$X = E \times \Delta t. \tag{1}$$

The CCD or CMOS sensor produces electrical signals proportional to the sensor exposure X. These electrical signals are sampled and quantized by the analog-to-digital converter (ADC) to generate digital signals. Usually, the ADC output is further remapped to fit for certain purposes, like gamma correction. Typically, the overall effect of the image sensor, ADC, and the remapping function can be integrated and approximated as a nonlinear transfer function $g(\ )$, named the CRF. With this approximation, the digital value D at a pixel can be expressed as

$$D = g(X) = g(E \times \Delta t). \tag{2}$$

In general, in the capturing of an RGB color image, different color channels may have different CRF functions. To simplify

the problem, we assume the CRF functions for all three color channels are roughly the same. Indeed, some camera manufactures may tend to have different CRF functions for their cameras. Under such a situation, the colors of the enhanced images would be somewhat different from the colors in the well-illuminated images captured by the real cameras. However, since our major focus is the improvement of the luminance contrast, we still adopt the same-CRF assumption in our algorithm to simplify the problem. In the following deductions and simulation, we convert an RGB image into an HSI format and focus on the I (intensity) component only.

The pixel-wise relationship in (2) can be further extended to model the relation between the digital values over an image patch and their corresponding irradiance values. Here, we denote $\vec{d}_\ell$ as the 1-D vector representation of the digital values over an image patch and $\vec{E}_\ell$ as the 1-D vector representation of the corresponding irradiance values. Over a local patch, the nonlinear mapping in (2) can be approximated as a first-order mapping function, as long as the values of X within the patch do not span a very wide range. That is, we approximate $\vec{d}_\ell$ as

$$\vec{d}_\ell \approx a \cdot \vec{E}_\ell + b \cdot \vec{1} \tag{3}$$

where $\vec{1}$ is a 1-D vector that has the same dimension as $\vec{E}_\ell$ and has all elements equal to 1. If subtracting the local mean from $\vec{d}_\ell$ and $\vec{E}_\ell$, we have

$$\vec{d}_\ell - d_{\ell,m} \cdot \vec{1} \approx a \cdot (\vec{E}_\ell - E_{\ell,m} \cdot \vec{1}) \tag{4}$$

where $d_{\ell,m}$ and $E_{\ell,m}$ are the mean of the elements in $\vec{d}_\ell$ and $\vec{E}_\ell$, respectively. Equation (4) implies that there exists a collinear property between $(\vec{d}_\ell - d_{\ell,m} \cdot \vec{1})$ and $(\vec{E}_\ell - E_{\ell,m} \cdot \vec{1})$. With this collinear property, we propose the following constraint:

$$|\vec{E}_\ell - E_{\ell,m} \cdot \vec{1}| \cdot |\vec{d}_\ell - d_{\ell,m} \cdot \vec{1}| \approx (\vec{E}_\ell - E_{\ell,m} \cdot \vec{1}) \bullet (\vec{d}_\ell - d_{\ell,m} \cdot \vec{1}) \tag{5}$$

where "$|\ \ |$" denotes the l_2 norm and "$\bullet$" denotes the inner product operator. This equation indicates that the image structures of $\vec{E}_\ell$ and $\vec{d}_\ell$ would be quite similar for most local patches in the given image.

On the other hand, for the same sensor irradiance E, different camera settings may produce images of different visual quality, as illustrated in Fig. 2. In this example, with different shutter speeds, we obtain one dimly exposed image $d(x, y)$ and one brightly exposed image $f(x, y)$. Since the local image structures of these two images come from the same sensor irradiance $E(x, y)$, an image patch d_ℓ on $d(x, y)$ and its counterpart patch f_ℓ on $f(x, y)$ should share a similar structure. That is, we have

$$|\vec{f}_\ell - f_{\ell,m} \cdot \vec{1}| \cdot |\vec{d}_\ell - d_{\ell,m} \cdot \vec{1}| \approx (\vec{f}_\ell - f_{\ell,m} \cdot \vec{1}) \bullet (\vec{d}_\ell - d_{\ell,m} \cdot \vec{1}) \tag{6}$$

where $\vec{f}_\ell$ and $\vec{d}_\ell$ denote the 1-D vector representations of f_ℓ and d_ℓ, respectively.

However, for a smooth image patch, the collinear constraint degenerates. In this case, the value of $\vec{d}_\ell - d_{\ell,m} \cdot \vec{1}$ is approximately zero and any realization of $\vec{f}_\ell$ can satisfy the equality in (6). To deal with this problem, we further modify the constraint in (6) as

$$\begin{aligned} &|\vec{f}_\ell - f_{\ell,m} \cdot \vec{1} + c \cdot \vec{1}| \cdot |\vec{d}_\ell - d_{\ell,m} \cdot \vec{1} + c \cdot \vec{1}| \\ &\approx (\vec{f}_\ell - f_{\ell,m} \cdot \vec{1} + c \cdot \vec{1}) \bullet (\vec{d}_\ell - d_{\ell,m} \cdot \vec{1} + c \cdot \vec{1}) \end{aligned} \tag{7}$$

where c is a small constant value.

To verify the applicability of (7), we tested eight image pairs. In Fig. 3(a), we show two of these pairs. For each image pair, pictures of the same scene with two different camera settings are captured to get different luminance levels. For each image pair, by treating a 3×3 local patch in one image as $\vec{f}_\ell$ and its counterpart in the other image as $\vec{d}_\ell$, we compute the value of $S(\vec{f}_\ell, \vec{d}_\ell)$, which is defined as

$$S(\vec{f}_\ell, \vec{d}_\ell) \equiv \frac{|\vec{f}_\ell - f_{\ell,m} \cdot \vec{1} + c \cdot \vec{1}| \cdot |\vec{d}_\ell - d_{\ell,m} \cdot \vec{1} + c \cdot \vec{1}| - (\vec{f}_\ell - f_{\ell,m} \cdot \vec{1} + c \cdot \vec{1}) \bullet (\vec{d}_\ell - d_{\ell,m} \cdot \vec{1} + c \cdot \vec{1})}{|\vec{f}_\ell - f_{\ell,m} \cdot \vec{1} + c \cdot \vec{1}| \cdot |\vec{d}_\ell - d_{\ell,m} \cdot \vec{1} + c \cdot \vec{1}|}. \tag{8}$$

In (8), we normalize the numerator term over $|\vec{f}_\ell - f_{\ell,m} \cdot \vec{1} + c \cdot \vec{1}| \cdot |\vec{d}_\ell - d_{\ell,m} \cdot \vec{1} + c \cdot \vec{1}|$ to deal with images of different sizes or of different bit-lengths. In Fig. 3(b), we show the histogram of $S(\vec{f}_\ell, \vec{d}_\ell)$ for one image pair. As expected, the histogram shape is roughly an exponentially decreasing function peaked at zero. In Table I, we list the mean and standard deviation of the histogram $S(\vec{f}_\ell, \vec{d}_\ell)$ for each of the eight image pairs. This experiment demonstrates that (7) is indeed a feasible constraint to link images of different exposures.

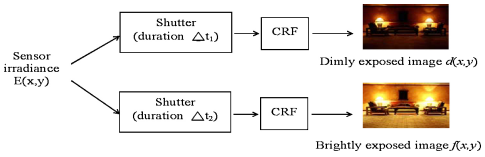

Fig. 2. Camera settings versus image quality.

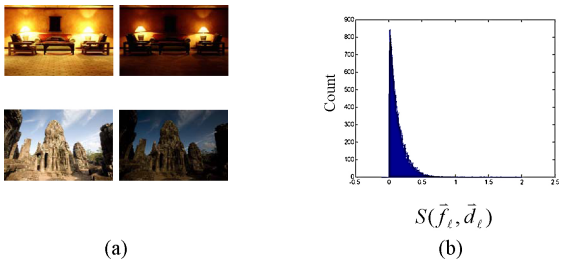

Fig. 3. (a) Image pairs with two different luminance levels. (b) Histogram of $S(\vec{f}_\ell, \vec{d}_\ell)$ with $c = 1$.

B. Bayesian Framework

In this paper, given a poorly exposed image $\boldsymbol{d}$, we aim to infer a well-exposed image $\boldsymbol{f}$ by maximizing a properly designed posterior probability function $p(\boldsymbol{f}/\boldsymbol{d})$. Mathematically, we have

$$\boldsymbol{f}^* = \arg\max_{\boldsymbol{f}} p(\boldsymbol{f}|\boldsymbol{d}) \tag{9}$$

TABLE I
MEAN AND STANDARD DERIVATION OF $S(\vec{f}_\ell, \vec{d}_\ell)$

	Mean	Standard Deviation
Image pair 1	0.2431	0.2265
Image pair 2	0.2808	0.3150
Image pair 3	0.2146	0.2249
Image pair 4	0.2875	0.2937
Image pair 5	0.3261	0.2590
Image pair 6	0.1281	0.1168
Image pair 7	0.2655	0.2577
Image pair 8	0.1875	0.2054

$$\text{or} \qquad \boldsymbol{f}^* = \arg\max_{f}\{p(\boldsymbol{d}|\boldsymbol{f})p(\boldsymbol{f})\}. \tag{10}$$

In (10), $p(\boldsymbol{d}|\boldsymbol{f})$ is the likelihood model that represents the relationship between the observed image $\boldsymbol{d}$ and the desired image $\boldsymbol{f}$. $p(\boldsymbol{f})$ is the prior model that describes some expected statistical properties of the desired image. In our approach, we construct the likelihood model based on the aforementioned constraint in Section II-A. That is

$$p(\boldsymbol{d}|\boldsymbol{f}) \propto \exp\{-w_\ell \cdot \sum_i [|\vec{f}_{i,\ell} - f_{i,m}\vec{1} + c\vec{1}| \cdot |\vec{d}_{i,\ell} - d_{i,m}\vec{1} + c\vec{1}| - (\vec{f}_{i,\ell} - f_{i,m}\vec{1} + c\vec{1}) \bullet (\vec{d}_{i,\ell} - d_{i,m}\vec{1} + c\vec{1})]^r\}. \tag{11}$$

In (11), i denotes the pixel index, $\vec{d}_{i,\ell}$ is the 1-D vector representation of the $p \times p$ image patch centered at pixel i, $\vec{f}_{i,\ell}$ is the 1-D vector representation of the $p \times p$ desired image patch centered at pixel i, $f_{i,m}$ and $d_{i,m}$ are the mean of the elements in $\vec{f}_{i,\ell}$ and $\vec{d}_{i,\ell}$, and w_ℓ is a weighting factor to control the influence of the likelihood model. Moreover, r is a parameter for the shape control of the likelihood model. With (11) we aim to reconstruct an image $\boldsymbol{f}$ whose local structures are similar to that of the observed image $\boldsymbol{d}$. In our algorithm, the actual size of the observed image patch is 3×3 and the value of r is empirically chosen to be 1.8.

As mentioned above, the use of the constant c in (11) is to deal with flat regions. However, this constant term may also affect the degree of the enhancement level. Consider two edge intensity profiles in Fig. 4, where the black profile indicates a mean-subtracted input profile $\hat{d}$ while the red profile indicates the desired mean-subtracted profile $\hat{f}$. Here, we denote the dynamic range of $\hat{d}$ and $\hat{f}$ as $[d_{\min}, d_{\max}]$ and $[f_{\min}, f_{\max}]$, respectively. If the constant term c is set to 0, the relationship between $\hat{d}$ and $\hat{f}$ would be $\hat{f} \approx \alpha \cdot \hat{d}$ for some positive value α, with

$$\alpha < \min\{\frac{f_{\max}}{d_{\max}}, \frac{f_{\min}}{d_{\min}}\}. \tag{12}$$

Please note that both $d_{\min}$ and $f_{\min}$ are negative. With the inclusion of c, the range of α becomes

$$\begin{cases} \alpha < \min\{\frac{f_{\max}}{d_{\max}+c}, \frac{f_{\min}}{d_{\min}+c}\}, & \text{if } -d_{\max} < c < -d_{\min} \\ \alpha < \frac{f_{\max}}{d_{\max}+c}, & \text{if } c \geq -d_{\min} \\ \alpha < \frac{f_{\min}}{d_{\min}+c}, & \text{if } c \leq -d_{\max}. \end{cases} \tag{13}$$

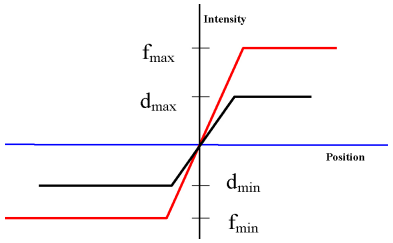

Fig. 4. Illustration of enhancement level.

Hence, by changing the value of c, the maximally allowed level of contrast enhancement is changed.

On the other hand, the prior model $p(\boldsymbol{f})$ of our Bayesian framework is designed to satisfy some statistical properties of a well-exposed image $\boldsymbol{f}$. Here, we design the image prior to satisfy two objectives: to enhance the visibility of true image details and to prevent the amplification of image noise. In our approach, we decompose the image prior into the product of two components: the enhancement prior $p_e(\boldsymbol{f})$ and the natural image prior $p_n(\boldsymbol{f})$. That is, we have

$$p(\boldsymbol{f}) = p_e(\boldsymbol{f})p_n(\boldsymbol{f}). \tag{14}$$

The role of $p_e(\boldsymbol{f})$ is to enhance the visibility of image details, while the role of $p_n(\boldsymbol{f})$ is to suppress noise amplification. Here, with a Markov random field model, we define $p_e(\boldsymbol{f})$ as

$$p_e(\boldsymbol{f}) \propto \exp(w_e \cdot \sum_i (w_i \cdot (\nabla^2 f_i)^2)). \tag{15}$$

In (15), w_e is a weighting factor to control the influence of the prior $p_e(\boldsymbol{f})$ and w_i is a data-dependent gain function that will be explained later. Besides, ∇^2 represents the Laplacian operator and $\nabla^2 f_i$ is the Laplacian response of the desired image $\boldsymbol{f}$ at pixel i. This prior definition prefers a realization of $\boldsymbol{f}$ with a strong Laplacian response. Since image details are highly correlated with the Laplacian response, the introduction of $p_e(\boldsymbol{f})$ can effectively enhance image details. Even though the Laplacian operation may cause undesirable ringing artifacts around strong edges, these ringing artifacts can be properly suppressed by the structure-preserving constraint in (11) and the natural image prior $p_n(\boldsymbol{f})$. In our system, the Laplacian filter has a 3×3 kernel, with the central coefficient being 1 while the other coefficients being $-1/8$.

In (15), the weight w_i is defined as

$$w_i = \exp(-\frac{|\nabla^2 d_i|}{A}) \cdot \exp(-\frac{d_{i,m}}{B}) \quad A, B > 0. \tag{16}$$

Here, A and B are two controlling parameters. $\nabla^2 d_i$ is the Laplacian response of the original image at pixel i. At a pixel with a small Laplacian response and a small intensity mean, we assign a large value of w_i, and vice versa. This design is to provide weaker enhancement for salient features in the observed image $\boldsymbol{d}$ while providing stronger enhancement over tiny features, especially over these features in dark regions.

On the other hand, in the design of $p_n(\boldsymbol{f})$, we adopt the field of expert (FoE) prior proposed in [31] which has the following

form to model the pdf of a noise-free natural image:

$$p_n(\boldsymbol{f}) \propto \exp(w_n \cdot \sum_{k \in S'} \sum_{z=1}^{N} \log \phi(J_z^T f_{C_k}; \alpha_z)) \tag{17}$$

with

$$\phi(J_z^T f_{C_k}; \alpha_z) \equiv [1 + \frac{1}{2}(J_z^T f_{C_k})^2]^{-\alpha_z}. \tag{18}$$

In (17), w_n is a weight that controls the influence of the prior $p_n(\boldsymbol{f})$, the clique C_k includes $n \times n$ pixels centered at pixel k, fc_k denotes the local image data over the clique C_k, J_z^T is a filter of size $n \times n$, and $J_z^T f_{C_k}$ is the inner product between the filter kernel and the local image data. Besides, N is the number of filters used in the modeling of $p_n(\boldsymbol{f})$. S' is a set containing all the center pixels of the $n_1 \times n_1$ cliques that fully overlap with the image support. Finally, α_z is a positive parameter that makes ϕ a proper distribution. A major property of the FoE prior is its use of the Student's t-distribution to describe the statistical distribution of noise-free natural images. Since ringing artifacts and image noise do not satisfy the characteristics of noise-free natural images, we can effectively suppress undesirable noise with the inclusion of the FoE prior. Besides, except w_n, all filters and parameters defined in (17) and (18) are learned from natural images. The training data of the FoE model were taken from 50 images in the Berkeley segmentation database. The FoE model was trained based on 2000 randomly cropped image regions with the width and height three times that of the cliques. More details about the learning of the FoE prior can be found in [31].

C. Bayesian Contrast Enhancement

Substituting the aforementioned likelihood model and prior model into the negative logarithm of (10), we get the following optimization formula for contrast enhancement:

$$\begin{aligned}
&\hat{\boldsymbol{f}} = \arg\min_{f}\{C(\boldsymbol{f})\} \quad \text{with} \\
&C(\boldsymbol{f}) \equiv w_\ell \cdot \sum_i (|\vec{f}_{i,\ell} - f_{i,m}\vec{1} + c\vec{1}| \cdot |\vec{d}_{i,\ell} - d_{i,m}\vec{1} + c\vec{1}| - \\
&\qquad (\vec{f}_{i,\ell} - f_{i,m}\vec{1} + c\vec{1}) \bullet (\vec{d}_{i,\ell} - d_{i,m}\vec{1} + c\vec{1}))^r \\
&\quad - w_e \cdot \sum_i (w_i \cdot (\nabla^2 f_i)^2) - w_n \cdot \sum_{k \in S'} \sum_{z=1}^{N} \log \phi(J_z^T f_{C_k}; \alpha_z) \\
&\quad = w_\ell \cdot C_\ell(\boldsymbol{f}) - w_e \cdot C_e(\boldsymbol{f}) - w_n \cdot C_n(\boldsymbol{f}).
\end{aligned} \tag{19}$$

In (19), we aim to find a realization of $\boldsymbol{f}$ whose local structure is similar to that of the original image, but with enhanced contrast. By changing the parameter setting, we can achieve different levels of contrast enhancement. In fact, (19) can also be interpreted as a regularized image restoration formulation, with the first term being a fidelity metric that measures the similarity between the original data and the restored data while the remaining terms being a regularizer that defines the behavior of the solution. Here, we model the relationship in an indirect way that avoids the need to exactly specify the unknown camera settings, like shutter speed and camera response function. Moreover, we include two kinds of prior information to provide improved enhancement results. Here, for convenience, we name our approach as Bayesian structure-preserving image contrast enhancement (BSPICE) algorithm. Moreover, we adopt the algorithm developed by Schmidt *et al.* [34] to find the optimal solution of (19).

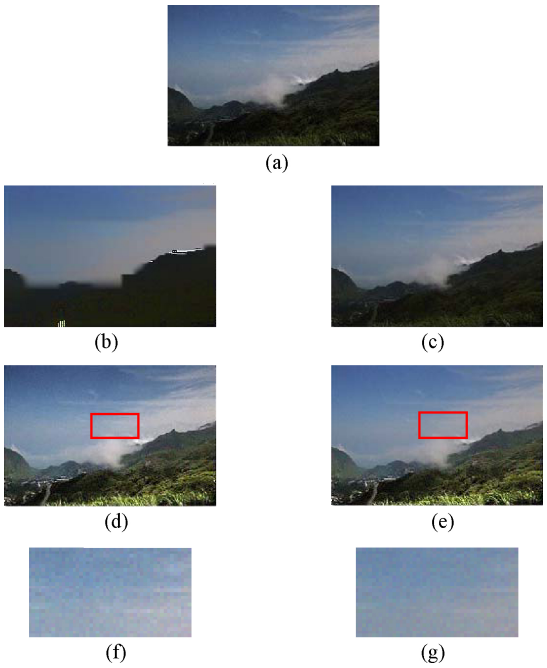

Fig. 5. Enhancement results with different settings of w_l, w_e, and w_n. (a) Original image. (b) Reconstructed image without the likelihood model $C_\ell(f)$. (c) Reconstructed image without the enhancement prior $C_e(\boldsymbol{f})$. (d) Reconstructed image without the natural image prior $C_n(\boldsymbol{f})$. (e) Reconstructed image with all $C_\ell(f)$, $C_e(\boldsymbol{f})$, and $C_n(\boldsymbol{f})$. (f) Enlarged red rectangular region in (d). (g) Enlarged red rectangular region in (e).

D. Simulation Result of BSPICE Algorithm

In this section, we will show some simulation results of the BSPICE algorithm. In Fig. 5, we illustrate the effect of the proposed likelihood model and prior models. The first case is to discard the likelihood model $C_\ell(f)$ during the reconstruction process. For the case, the enhancement process relies only on the prior knowledge $C_e(\boldsymbol{f})$ and $C_n(\boldsymbol{f})$. Under such situation, the enhancement process is similar to the combination of a high-frequency component and a smoothed image, as shown in Fig. 5(b). In the second case, we discard the enhancement prior $C_e(\boldsymbol{f})$ and only keep the other two. For this case, with the influence of the natural image prior $C_n(\boldsymbol{f})$, the enhancement process is similar to an image smoother, as shown in Fig. 5(c). In the third case, we discard the natural image prior $C_n(\boldsymbol{f})$ while keeping the other two. In this case, the enhancement result becomes more noisy, as shown in Fig. 5(d) and (f). For reference, we also show the enhancement results based on all three models in Fig. 5(e) and (g).

Moreover, in the construction of the constrained optimization problem in (19), the likelihood model $C_\ell(f)$ is constructed from the view point of image acquisition pipeline. Since the image acquisition process is independent of image contents, the deduced model can be successfully applied to various kinds of images. On the other hand, the natural image prior $C_n(\boldsymbol{f})$ is trained from 50 natural images in the Berkeley

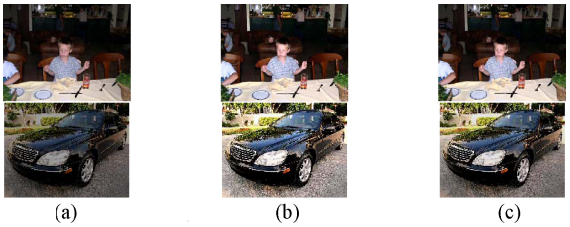

Fig. 6. Comparison of enhancement results with different c values. (a) Original image. (b) Enhanced image with $c = 2$. (c) Enhanced image with $c = 3$.

TABLE II
DEFAULT PARAMETER SETTINGS OF THE BSPICE ALGORITHM

Parameter	w_ℓ	w_e	w_n	c	A	B	r
Value	7	10	100	1.5	15	150	1.8

segmentation database. In our experiments, this natural image prior can be well applied to various kinds of images. Finally, the Laplacian operation used in the enhancement prior $C_e(\boldsymbol{f})$ is a popular methodology that can be used to enhance various kinds of images. Since all these three models in the constrained optimization problem are not image-dependent, the proposed BSPICE algorithm is expected to work well even for untrained images.

In the above experiments, we have demonstrated the influence of $C_\ell(f)$, $C_n(\boldsymbol{f})$, and $C_e(\boldsymbol{f})$. In Fig. 6, we further demonstrate the influence of the parameter c of the likelihood model over the degree of contrast enhancement. As expected, when the value of c is increased, the degree of contrast enhancement is lowered.

In Figs. 7 and 8, we compare the enhancement results of several image enhancement algorithms. Here, we pick the original histogram equalization algorithm, the bi-histogram algorithm (BHE) in [4], the DCT-based method in [23], and the multi-scale retinex (MSR) method in [17]. Actually, for the DCT-based approach in [23], the authors proposed three variants for contrast enhancement, with the short names TW-CES-BLK, DRC-CES-BLK, and SF-CES-BLK, respectively. The main difference among these three variants is the use of different intensity mapping functions for the adjustment of the DC component. In our simulation, the parameters in these algorithms were set to the default values suggested by the authors [4], [17], [23]. For a fair comparison with these algorithms, we fix the parameter setting of our BSPICE algorithm to the default values as listed in Table II.

As shown in Figs. 7 and 8, the proposed BSPICE method provides effective and natural-looking enhancement results for two different cases. In comparison, the results of HE are overly enhanced; the results of BHE are somewhat restricted due to the use of the mean-preserving constraint; the results of TW-CES-BLK, DRC-CES-BLK, and SF-CES-BLK may include apparent blocking artifacts. Besides, since the intensity mapping function for DC image modification in [23] is not content-dependent, some image features may not get properly enhanced. On the other hand, some undesirable ringing artifacts may become apparent in the results enhanced by MSR, like the area around the crest lines in Fig. 7(g).

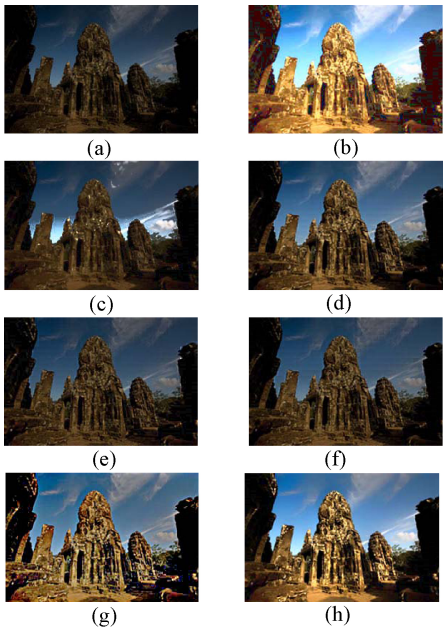

Fig. 7. Comparison of enhancement results. (a) Original image. (b) Histogram equalization. (c) Bi-histogram equalization method [4]. (d) TW-CES-BLK [23]. (e) DRC-CES-BLK [23]. (f) SF-CES-BLK [23]. (g) MSR [17]. (h) Proposed method.

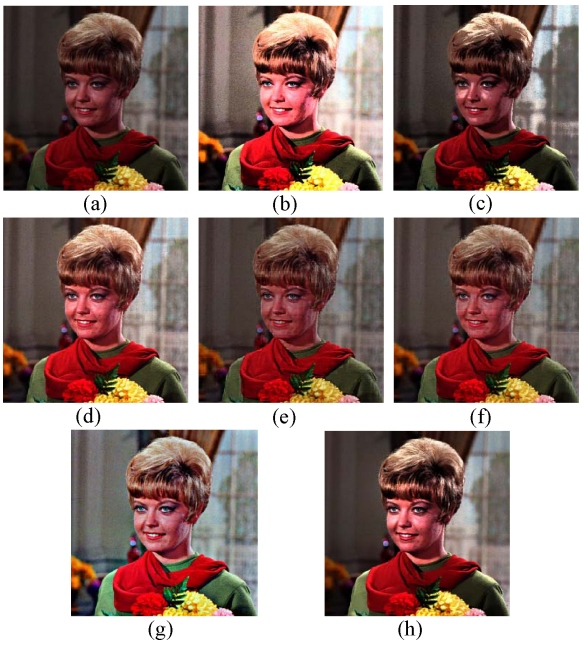

Fig. 8. Comparison of enhancement results. (a) Original image. (b) Histogram equalization. (c) Bi-histogram equalization method [4]. (d) TW-CES-BLK [23]. (e) DRC-CES-BLK [23]. (f) SF-CES-BLK [23]. (g) MSR [17]. (h) Proposed method.

Besides subjective evaluation, we also do the comparison based on three kinds of objective quality assessments: discrete entropy E_{np}, Brenner's measure (F_{br}) [26], and the measure of enhancement (EME) [35]. These three measures are defined as

$$E_{np} = -\sum_{L=0}^{255} p(L)\log_2 p(L) \tag{20}$$

TABLE III
DISCRETE ENTROPY E_{np}

	Image 1 (Fig. 7)	Image 2 (Fig. 8)	Image 3	Image 4
HE	6.43	6.93	6.48	6.88
BHE	6.47	7.24	6.65	6.92
TW-CES-BLK	6.94	7.58	7.21	7.39
DRC-CES-BLK	6.53	6.99	6.82	6.90
SF-CES-BLK	6.53	7.19	6.96	7.10
MSR	6.94	7.52	7.39	7.20
BSPICE	7.44	7.47	7.30	7.20

$$F_{br} = \sum_x \sum_y (I(x, y) - I(x+2, y))^2 \tag{21}$$

and

$$EME = \frac{1}{k_1 k_2} \sum_{l=1}^{k_2} \sum_{k=1}^{k_1} 20 \ln \frac{I^w_{\max;k,l}}{I^w_{\min;k,l} + con}. \tag{22}$$

In the above definitions, $p(L)$ is the normalized histogram bin count at level L and $I(x, y)$ is the intensity value of the image at (x, y). In (22), *con* is a small constant to avoid division-by-zero and the input image I is broken up into k_1 by k_2 nonoverlapping blocks. For the block with the indices (k, l), $I^w_{\max;k,l}$ and $I^w_{\min;k,l}$ indicate its maximum and minimum intensity values, respectively. In our experiment, the block size is chosen to be 8×8 and *con* is chosen to be 0.0001. Among these metrics, the discrete entropy is used to evaluate the uniformity of the intensity histogram; the Brenner's measure is used for sharpness assessment; and the EME value is an approximation of the averaged contrast in the image. Generally speaking, an image with higher values of E_{np}, F_{br}, and *EME* would have better visual quality. In Tables III–V, we summarize the assessment results over four different images. We can find that the MSR algorithm and our BSPICE algorithms produce higher values of E_{np}, F_{br} and *EME* in most cases. This is reasonable since both approaches perform contrast enhancement in a local, adaptive manner. Nevertheless, the proposed BSPICE algorithm generates fewer ringing artifacts and less color shift if compared with the MSR algorithm.

In the above experiments, we have adopted the default parameter setting listed in Table II for performance evaluation. Actually, in practical applications, we may want to fine-tune these parameters based on image contents or user preference. In Table VI, we list a few empirical rules as the guideline of parameter selection. In our BSPICE algorithm, to simplify the control of parameters, we fix w_e, w_n, r, and B while allowing w_ℓ, c, and A to vary based on image contents or user preference. In Fig. 9, we show two examples of enhancement results based on the default setting and the fine-tuned setting, respectively. For the upper image in Fig. 9(c), we choose $w_\ell = 7$, $c = 1.5$, and $A = 20$. For the lower image, we choose $w_\ell = 7$, $c = 1.2$, and $A = 20$.

In the proposed BSPICE algorithm, we obtain the enhanced image based on the optimization of (19). It would be interesting to see what would happen if we apply the optimization of (19) once again over the already enhanced image. In Fig. 10, we show two examples of enhancement results in which we

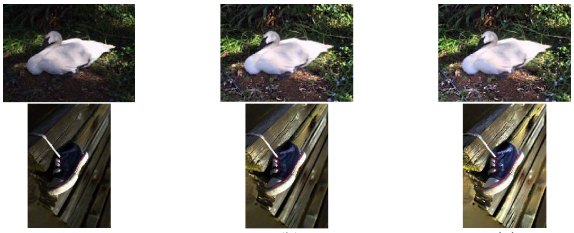

(a) (b) (c)

Fig. 9. Enhancement results with different parameter settings. (a) Original image. (b) Default settings. (c) Fine-tuned settings.

TABLE IV
BRENNER'S MEASURE F_{br} (UNIT: 10^6)

	Image 1 (Fig. 7)	Image 2 (Fig. 8)	Image 3	Image 4
HE	56.12	48.57	88.66	32.17
BHE	21.51	32.41	34.13	30.98
TW-CES-BLK	26.74	30.10	38.63	28.85
DRC-CES-BLK	16.18	17.66	29.70	24.15
SF-CES-BLK	17.00	19.59	31.05	25.24
MSR	86.99	36.56	65.26	44.53
BSPICE	70.80	36.34	43.30	35.84

TABLE V
EME VALUE

	Image 1 (Fig. 7)	Image 2 (Fig. 8)	Image 3	Image 4
HE	18.53	41.50	81.11	45.03
BHE	62.84	35.69	75.40	42.54
TW-CES-BLK	83.46	19.16	48.57	19.36
DRC-CES-BLK	85.43	19.02	49.52	19.89
SF-CES-BLK	82.68	19.19	48.53	19.88
MSR	96.39	21.23	68.12	28.09
BSPICE	99.36	40.01	81.61	47.58

TABLE VI
EMPIRICAL GUIDELINES FOR PARAMETER ADJUSTMENT

Parameter	Description
w_ℓ	A small w_ℓ is preferred for low-SNR images. The suggested range for w_ℓ is 1–10.
w_e	A larger value of w_e is required for poorly illuminated images. The default value for w_e is 10.
w_n	A large value of w_n is required for a noisy image or an under-exposed image. The default value for w_n is 100.
c	A parameter to control enhancement degree. A smaller value of c is preferred for a poorly illuminated image. The suggested range for c is 1–3.
A	A smaller value of A causes weaker enhancement for salient features while stronger enhancement over tiny features. The suggested range for A is 10–40.
B	A smaller value of B causes weaker enhancement for features in the bright regions while stronger enhancement for features in dark regions. The default value for B is 150.
r	A small value of r is preferred for low-SNR images. The default value for r is 1.8.

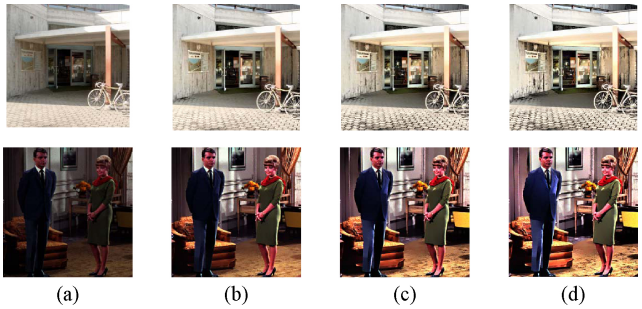

Fig. 10. Enhanced images after repeatedly applying the BSPICE algorithm. (a) Original image. (b) One-time enhancement. (c) Two-time enhancement. (d) Four-time enhancement.

apply the BSPICE algorithm several times based on the default parameter setting. These two examples show that the images may get somewhat overly enhanced as we repeatedly apply the BSPICE algorithm to the enhanced image. This phenomenon is expectable since the default parameter setting that is suitable for low-contrast images may not work well for images of higher contrast.

III. Simplified BSPICE Algorithm

In Section II, we present a Bayesian framework for contrast enhancement. However, since we need to estimate $M \times N$ unknown variables for an $M \times N$ image, directly solving (19) would be extremely time-consuming. In this section, we further propose a simplified Bayesian framework to greatly alleviate the computational complexity of the BSPICE algorithm.

First, from the viewpoint of image acquisition, the relationship between f_i and d_i can be described by a simple mapping function. See Fig. 2 for example, f_i and d_i would roughly satisfy the following equation:

$$f_i = g\left(\frac{\Delta t_2}{\Delta t_1} g^{-1}(d_i)\right) = G(d_i) \tag{23}$$

where $g^{-1}(\ )$ represents the inverse of the camera response function. This equation indicates that the relationship between f_i and d_i can be expressed in terms of a mapping function $G(\ )$, which is highly related to the camera response function. Second, with the use of the structure-preserving constraint in the BSPICE algorithm, we expect the original data d_i could be roughly related with the enhanced data f_i in terms of a mapping function, in spite of the fact that the optimization of (19) is actually a pixel-wise process. To test this supposition, we check the joint distribution $Dist(f_i, d_i)$ over a few image pairs. Take the original image in Fig. 11(a) as an example, we show its BSPICE-enhanced image in Fig. 11(b). In Fig. 11(c), we show the joint distribution $Dist(f_i, d_i)$ between these two images. In this figure, the value of $Dist(f_i, d_i)$ is represented in pseudocolors, with blue color for smaller values, yellow color for middle values, and red color for large values. This figure demonstrates that the relationship between f_i and d_i can be roughly approximated by a single mapping function. We have tested a few other image pairs and have reached the same conclusion.

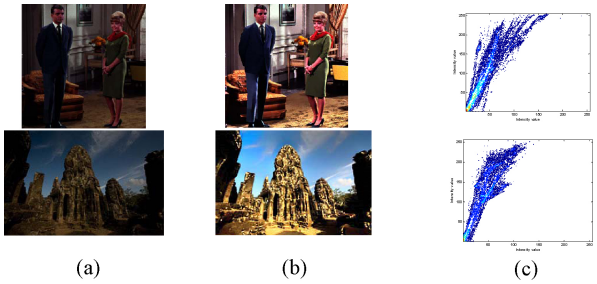

Fig. 11. (a) Dimly exposed image. (b) BSPICE-enhanced image. (c) Joint distribution.

Based on the above observation, we assume that the relationship between a poorly exposed image $\boldsymbol{d}$ and the enhanced image $\boldsymbol{f}$ can be represented by a monotonically increasing intensity transfer function T. That is, if d_i and f_i denote the intensity value at pixel i of $\boldsymbol{d}$ and $\boldsymbol{f}$, respectively, we have

$$f_i = T(d_i) \tag{24}$$

with $T'(d_i) \geq 0$. Even though the transfer function T can be defined for any value of d_i, actually we only care about the 256 discrete values of d_i for an 8-bit imaging system. That is, we focus only on the finding of the set $\mathbf{T} \equiv \{T(0), T(1), \ldots, T(255)\}$. Moreover, the monotonically increasing constraint can be expressed as a system of linear inequality equations

$$T(L) - T(L-1) \geq 0, \quad \text{where } L \in \{1, 2, \ldots, 255\}. \tag{25}$$

By combining (19), (24), (25), and the discrete transfer function assumption, we get the following constrained optimization formulation for enhancement:

$$\begin{aligned}\hat{\mathbf{T}} &= \arg\min_{\mathbf{T}}\{C(\mathbf{T})\} \quad \text{with} \\ C(\mathbf{T}) &\equiv \boldsymbol{w}_\ell \cdot \sum_i (|\vec{\boldsymbol{f}}_{i,\ell} - \boldsymbol{f}_{i,m}\vec{1} + \boldsymbol{c}\vec{1}| \cdot |\vec{\boldsymbol{d}}_{i,\ell} - \boldsymbol{d}_{i,m}\vec{1} + c\vec{1}| \\ &\quad - (\vec{\boldsymbol{f}}_{i,\ell} - \boldsymbol{f}_{i,m}\vec{1} + \boldsymbol{c}\vec{1}) \bullet (\vec{\boldsymbol{d}}_{i,\ell} - \boldsymbol{d}_{i,m}\vec{1} + \boldsymbol{c}\vec{1}))^r \\ &\quad - \boldsymbol{w}_e \cdot \sum_i (\boldsymbol{w}_i \cdot (\nabla^2 \boldsymbol{f}_i)^2) - \boldsymbol{w}_n \cdot \sum_{k \in S'} \sum_{z=1}^{N} \log \phi(\boldsymbol{J}_z^T \boldsymbol{f}_{C_k}; \boldsymbol{\alpha}_z)\end{aligned} \tag{26}$$

subject to

$$f_i = T(d_i) \tag{27}$$

$$0 \leq T(L) \leq 255 \tag{28}$$

and

$$T(L) - T(L-1) \geq 0 \tag{29}$$

$$\text{with } L \in \{0, 1, \ldots, 255\} \text{ and } T(-1) = 0.$$

By solving (26) with the constraints in (27)–(29), we can obtain the optimal $\mathbf{T}$ for contrast enhancement.

A. Efficient Solver for the Optimization Problem

The introduction of intensity transfer function greatly reduces the number of unknown variables from $M \times N$ variables in (19) down to 256 variables in (26). To solve the constrained optimization formula defined in (26)–(29), we adopt the projection methodology for the optimal solution [32]. The basic concept of the projection-based algorithm is to project an unfeasible solution into the constraint set via a proper projection operator Π. In our approach, the whole procedure for the optimal solution $\mathbf{T}$ is summarized as follows.

1) $k = 0$.
   Initialize the set $\mathbf{T}^0 \equiv \{T(0)^0, T(1)^0, \ldots, T(255)^0\}$ as $T(L)^0 = L$, for $L = 0, 1, \ldots, 255$.
2) Update $\mathbf{T}$ by the iterative algorithm
$$T(L)^{k+1} = T(L)^k + \mu_k \cdot S_d(T)|_{T=T^k} \tag{30}$$
   for $L = 0, 1, \ldots, 255$.
3) If the set $\mathbf{T^{k+1}}$ violates the constraint in (28) and (29), we refine $\mathbf{T^{k+1}}$ as
$$\mathbf{T^{k+1}} = \Pi[\mathbf{T^{k+1}}]. \tag{31}$$
4) We iteratively perform Steps 2 and 3 until the stopping criterion is satisfied.

In our simulation, the algorithm stops when any of the following criteria is satisfied:

1) the change of the cost function value between two successive steps is smaller than the preset threshold;
2) the norm of the search direction is smaller than the preset threshold;
3) the difference between the updated solution and current solution is smaller than the preset threshold.

Moreover, in our simulation, the threshold values in all cases are empirically set to 10^{-6}. This threshold value would determine the number of iterations. A larger threshold value usually leads to faster convergence.

In the proposed process, $T(L)^k$ is the feasible solution obtained at the kth step, μ_k is the step size which is obtained by the backtracking line search algorithm [34], $S_d(\mathbf{T})$ is the search direction at $\mathbf{T^k}$ which is highly related to the cost function $C(\mathbf{T})$ in (26), and Π is the operator that projects the original infeasible solutions $\mathbf{T}^{k+1}$ into the constraint set Ω defined by the intersection of (28) and (29).

Same as the BSPICE algorithm, the algorithm [34] is adopted for the solution update in (30). However, some other iterative algorithms can also be used for solution update. In [34], the gradient direction for the algorithm is defined as

$$\left(\frac{\partial C(\mathbf{T})}{\partial T(L)}\right)|_{\mathbf{T}=\mathbf{T}^k} = \sum_i \left(\frac{\partial C(f)}{\partial f_i}|_{f=\mathbf{T}^k(d)}\right)\frac{\partial f_i}{\partial T(L)}$$
$$= \sum_i \left(\frac{\partial C(f)}{\partial f_i}|_{f=\mathbf{T}^k(d)}\right) \cdot \delta[d_i - L]\ . \tag{32}$$

In (32), f_i denotes the intensity value of the desired image $\boldsymbol{f}$ at pixel i, and $\boldsymbol{f} = T^k(\boldsymbol{d})$ denotes the transformation of the observed image $\boldsymbol{d}$ based on the intensity transfer function $\mathbf{T^k}$. Besides, $\delta[n]$ is the delta function defined as

$$\delta[n] = \begin{cases} 1, & n = 0 \\ 0, & n \neq 0. \end{cases}$$

Moreover, $\frac{\partial C(f)}{\partial f_i}|_{f=\mathbf{T}^k(d)}$ is the partial derivative of $C(\boldsymbol{f})$ with respect to the pixel value f_i.

To design a suitable projection operator Π for the optimization problem, we convert $\mathbf{T}$ into the gradient domain, where the monotonically increasing constraint in (29) can be easily verified. Here, the gradient of $\mathbf{T}$ is defined as

$$\nabla T(L) = T(L) - T(L-1) \tag{33}$$

where L $\in \{0, 1, 2, \ldots, 255\}$ and $T(-1) = 0$. In the gradient domain, the monotonically increasing constraint in (29) is equivalent to

$$\nabla T(L) \geq 0 \qquad \text{where } L \in \{0, 1, 2, \ldots, 255\}. \tag{34}$$

On the other hand, the dynamic range constraint in (28) is reformulated as

$$\sum_{L=0}^{255}(T(L) - T(L-1)) = \sum_{L=0}^{255}\nabla T(L) = 255. \tag{35}$$

In our projection operator Π, we first convert $\mathbf{T}^{k+1}$into the gradient domain to get $\nabla\mathbf{T}^{k+1}$. The gradient $\nabla\mathbf{T}^{k+1}$ is projected onto the non-negative domain to get $\nabla\mathbf{T}_+^{k+1}$ that satisfies the monotonically increasing constraint in (34). $\nabla\mathbf{T}_+^{k+1}$ is further projected onto the constrained dynamic range domain to get $\nabla\mathbf{T}_{++}^{k+1}$ that satisfies the dynamic range constraint in (35). In detail, we define $\nabla\mathbf{T}_+^{k+1}$ as

$$\nabla T(L)_+^{k+1} = \begin{cases} \nabla T(L)^{k+1}, & \text{if } \nabla T(L)^{k+1} \geq 0 \\ 0, & \text{if } \nabla T(L)^{k+1} < 0 \end{cases} \text{for } L = 0, 1, \ldots, 255 \tag{36}$$

which is a Euclidean projection of $\nabla\mathbf{T}^{k+1}$onto the constraint set in (34) [33]. On the other hand, the conversion from $\nabla\mathbf{T}_+^{k+1}$ to $\nabla\mathbf{T}_{++}^{k+1}$ is formulated as a constrained least-squares problem

$$\nabla\mathbf{T}_{++}^{k+1} = \arg\min_{\nabla\mathbf{T}_{++}^{k+1}}\{\frac{1}{2}\sum_{L=0}^{255} w_L \cdot [\nabla T(L)_{++}^{k+1} - \nabla T(L)_+^{k+1}]^2\} \tag{37}$$

subject to

$$\sum_{L=0}^{255}\nabla T(L)_{++}^{k+1} = 255 \tag{38}$$

and

$$\begin{cases} \nabla T(L)_{++}^{k+1} = 0, & \text{if } \nabla T(L)_+^{k+1} = 0 \\ \nabla T(L)_{++}^{k+1} \geq 0, & \text{if } \nabla T(L)_+^{k+1} \geq 0. \end{cases} \tag{39}$$

The formulation of (37)–(39) is to find a modified gradient solution $\nabla T_{++}^{k+1} = \{\nabla T_{++}^{k+1}(0), \nabla T_{++}^{k+1}(1), ..., \nabla T_{++}^{k+1}(255)\}$ that minimizes the weighted Euclidean distance between ∇T_+^{k+1} and ∇T_{++}^{k+1} while satisfying the constraints defined in (38) and (39) at the same time. Moreover, if there are M nonzero elements in $\nabla\mathbf{T}_+^{k+1}$ and the set $\mathbf{S}_+ = \{\mathrm{S}_+(1), S_+(2), \ldots, S_+(\mathrm{M})\}$ denotes the collection of these nonzero elements, an interesting result can be obtained if we intentionally set the weight w_L in (37) to be

$$w_L = \begin{cases} \left[\frac{(\prod_{m=1}^{M} S_+(m))}{(\nabla T(L)_+^{k+1})^{M-1}}\right]^{\frac{1}{(M-1)}}, & \text{if } \nabla T(L)_+^{k+1} \neq 0 \\ 0, & \text{if } \nabla T(L)_+^{k+1} = 0. \end{cases} \tag{40}$$

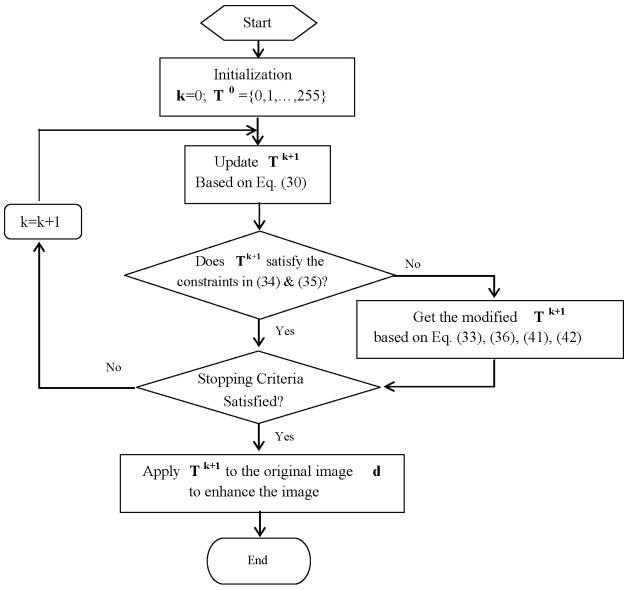

Fig. 12. Flow chart of the S-BSPICE algorithm.

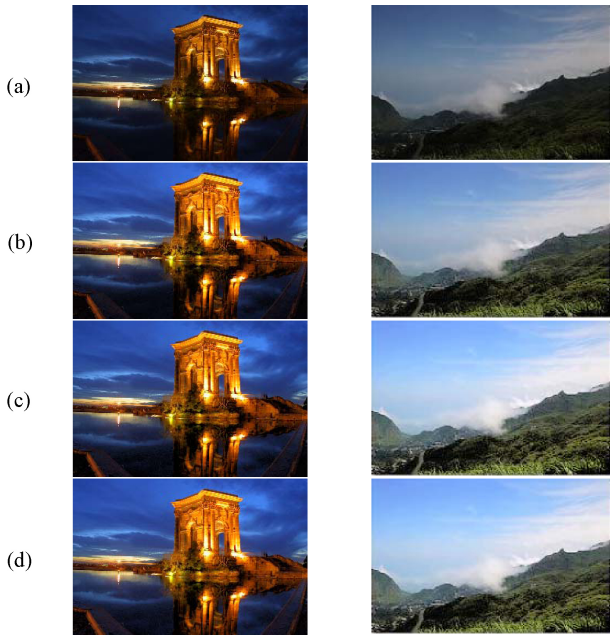

Fig. 13. Simulation results for S-BSPICE when iterations proceed. (a) Original image, and the processed images (b) after two iterations, (c) after six iterations, and (d) after the stopping criterion is satisfied (left image: 13 iterations, right image: 14 iterations).

With this setting, it can be shown that the solution of the constrained least-squares problem in (37)–(40) becomes

$$\nabla T_{++}^{k+1}(L) = 255 \cdot \frac{\nabla T_{+}^{k+1}(L)}{\sum_{j=0}^{255} \nabla_{+}^{k+1}(j)} \quad \text{for } L = 0, 1, \ldots, 255. \quad (41)$$

Finally, after the computation of ∇T_{++}^{k+1}, the refined $\mathbf{T^{k+1}}$ can be obtained by integrating the values of ∇T_{++}^{k+1}. That is

$$T(L)^{k+1} = \sum_{j=0}^{L} \nabla \mathbf{T}_{++}^{k+1}(j) \quad \text{for } L = 0, 1, \ldots, 255. \quad (42)$$

In summary, we propose a simplified algorithm that iteratively updates the set $\mathbf{T} = \{T(0), T(1), \ldots, T(255)\}$ as follows.

1) $k = 0$.
   Initialize the set $\mathbf{T}^0 \equiv \{T(0))^0, T(1)^0, \ldots, T(255))^0\}$ as $T(L)^0 = L$, for $L = 0, 1, \ldots, 255$.
2) Update $\mathbf{T}^k \equiv \{T(0)^k, T(1)^k, \ldots, T(255)^k\}$ by (30) for $L = 0, 1, \ldots, 255$.
3) If the set $\mathbf{T}^{k+1}$ violates the constraint defined in (28) and (29), we refine $\mathbf{T}^{k+1}$ as follows.
   a) Calculate $\nabla \mathbf{T}^{k+1}$, as defined in (33).
   b) Calculate $\nabla \mathbf{T}_{+}^{k+1}$, as defined in (36).
   c) Calculate $\nabla \mathbf{T}_{++}^{k+1}$, as defined in (41).
   d) Calculate the refined $\mathbf{T^{k+1}}$, as defined in (42).
4) Repeat Steps 2 and 3 until the stopping criterion is satisfied.

For the sake of convenience, the above procedure is named the S-BSPICE algorithm, which stands for the simplified BSPICE algorithm. For better understanding of the proposed algorithm, we also plot its process flow in Fig. 12.

B. Simulation Result of S-BSPICE Algorithm

In this section, we show some comparisons of the proposed S-BSPICE algorithm with a few existing algorithms. In the following simulation, the parameter settings of the S-BSPICE algorithm are basically the same as that in the BSPICE algorithm, except that the value of w_e is 50, and the value of w_ℓ is 1.9. Here, w_ℓ are assigned a smaller value due to the assumption of the global mapping function $\mathbf{T}$.

Differently from the BSPICE algorithm, the S-BSPICE algorithm is inherently an iterative process. In Fig. 13, we demonstrate the simulation results of the S-BSPICE algorithm. It can be easily seen that the enhancement performance gets improved as the iterations proceed.

Moreover, with S-BSPICE, the image quality usually gets improved up to a certain level in only a few iterations, long before the stopping criterion is reached. In our algorithm, an early-stopping strategy is evoked when the mean square error between two successive images is smaller than 8. In Fig. 14, we show two examples of early stop. This early-stopping strategy makes the S-BSPICE algorithm even more efficient in practical applications.

Figs. 15–17 demonstrate some simulation results of the S-BSPICE algorithm, in comparison with that of the HE algorithm, the BHE algorithm in [4], the DCT-based methods in [23], and the MSR algorithm in [17]. We can find that the proposed S-BSPICE algorithm provides impressive enhancement results, but with fewer artifacts. Moreover, even though the S-BSPICE algorithm actually performs global adjustment, it achieves enhancement performance comparable to that of local-adjustment approaches, like the MSR algorithm and the BSPICE algorithm.

In Tables VII–IX, we also summarize the objective assessment results over three different images Figs. 15–17. We can find that, in these cases, the S-BSPICE algorithm and the S-BSPICE algorithm with early-stopping produce similar E_{np},

Fig. 14. Simulation results for S-BSPICE with early-stopping strategy. (a) Original image, and processing images (b) with early-stopping (left image: three iterations, right image: three iterations), (c) after the stopping criterion is satisfied (left image: 101 iterations, right image: 13 iterations).

TABLE VII
DISCRETE ENTROPY E_{np}

	Fig. 15	Fig. 16	Fig. 17
HE	6.53	6.88	6.54
BHE	7.24	6.92	6.59
TW-CES-BLK	7.32	7.39	5.44
DRC-CES-BLK	7.41	6.90	6.49
SF-CES-BLK	7.29	7.10	6.35
MSR	7.22	7.20	6.50
BSPICE	7.13	7.20	6.71
S-BSPICE (reach the stopping criterion)	7.19	6.92	6.76
S-BSPICE (early-stopping)	7.10	6.89	6.61

TABLE VIII
BRENNER'S MEASURE F_{br} (UNIT: 10^6)

	Fig. 15	Fig. 16	Fig. 17
HE	129.81	32.17	102.12
BHE	142.55	30.98	53.36
TW-CES-BLK	212.20	28.85	8.54
DRC-CES-BLK	167.03	24.15	13.45
SF-CES-BLK	171.69	25.24	12.78
MSR	221.39	44.53	13.55
BSPICE	207.49	35.84	29.07
S-BSPICE (reach the stopping criterion)	126.54	20.92	32.48
S-BSPICE (early-stopping)	126.34	23.02	25.94

F_{br}, and *EME* values. This verifies the applicability of the early-stopping strategy in accelerating the original S-BSPICE algorithm.

It is also interesting to compare the simulation results of the BSPICE and S-BSPICE. Since BSPICE is basically a local processing, we can find that the processed results of BSPICE in Figs. 15–17 are better than that of S-BSPICE. However, since the dimensionality of the S-BSPICE algorithm is much smaller and only some simple operations, like clipping and rescaling, are involved, the execution time of S-BSPICE

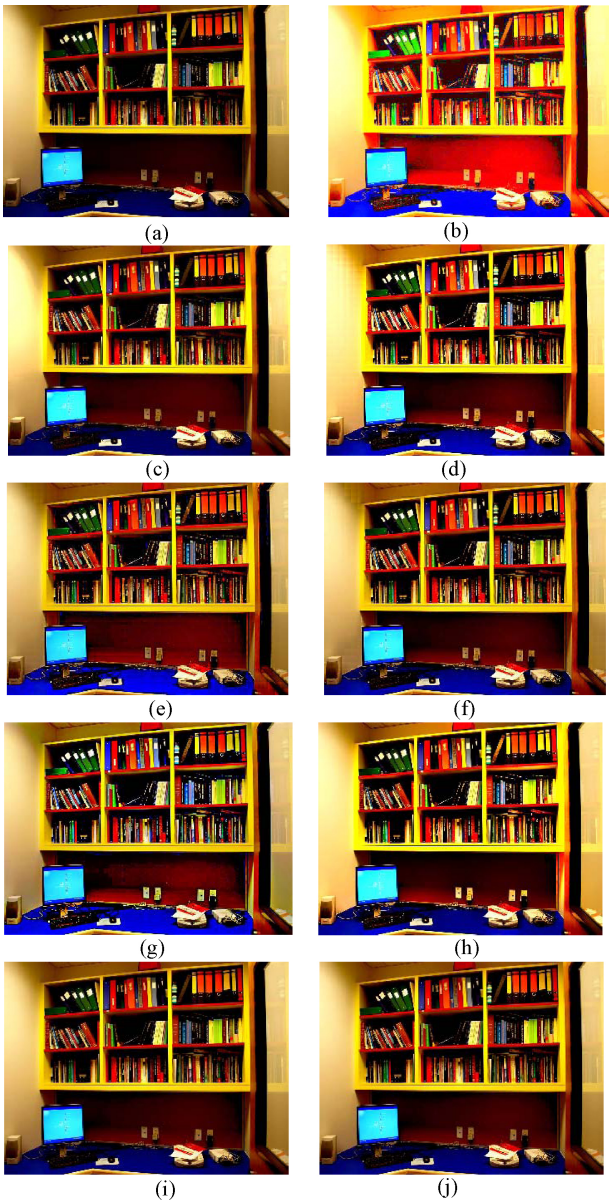

Fig. 15. Comparison of enhancement results. (a) Original image. (b) Histogram equalization. (c) Bi-histogram equalization method [4]. (d) TW-CES-BLK [23]. (e) DRC-CES-BLK [23]. (f) SF-CES-BLK [23]. (g) MSR [17]. (h) BSPICE. (i) S-BSPICE (early-stopping, three iterations). (j) S-BSPICE (nine iterations, stopping criterion is satisfied).

TABLE IX
EME VALUE

	Fig. 15	Fig. 16	Fig. 17
HE	22.50	45.03	52.73
BHE	91.91	42.54	13.23
TW-CES-BLK	111.98	19.36	3.19
DRC-CES-BLK	114.77	19.89	4.37
SF-CES-BLK	112.33	19.88	4.18
MSR	130.46	28.09	4.38
BSPICE	134.41	47.58	7.59
S-BSPICE (reach the stopping criterion)	118.35	41.13	8.06
S-BSPICE (early-stopping)	127.74	28.20	6.62

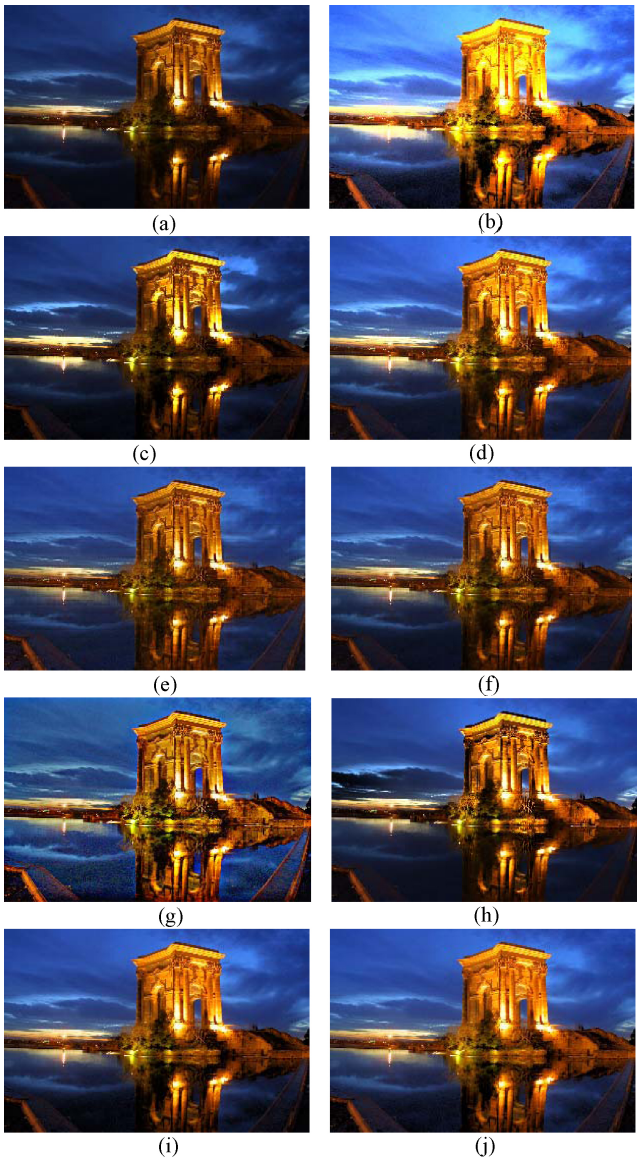

Fig. 16. Comparison of enhancement results. (a) Original image. (b) Histogram equalization. (c) Bi-histogram equalization method [4]. (d) TW-CES-BLK [23]. (e) DRC-CES-BLK [23]. (f) SF-CES-BLK [23]. (g) MSR [17]. (h) BSPICE. (i) S-BSPICE (early-stopping, three iterations). (j) S-BSPICE (13 iterations, stopping criterion is satisfied).

algorithm is a lot faster than BSPICE. In Table X, we list the comparison of execution time between BSPICE and S-BSPICE with early-stopping, together with the MATLAB implementation of the HE algorithm, the Bi-histogram equalization algorithm in [4], and the DCT-based methods in [23]. All algorithms are implemented using MATLAB on a desktop PC with an Intel Core i3 2.93 GHz CPU. Since the MSR simulation in our experiment is based on the PhotoFlair software developed by TruView Imaging Company whose source code is not available, the execution time of MSR is not included in Table X. As expected, the proposed BSPICE requires a much longer computation time. On the other hand, the S-BSPICE algorithm spends slightly longer computation time than the other algorithms, but with the tradeoff of improved visual quality.

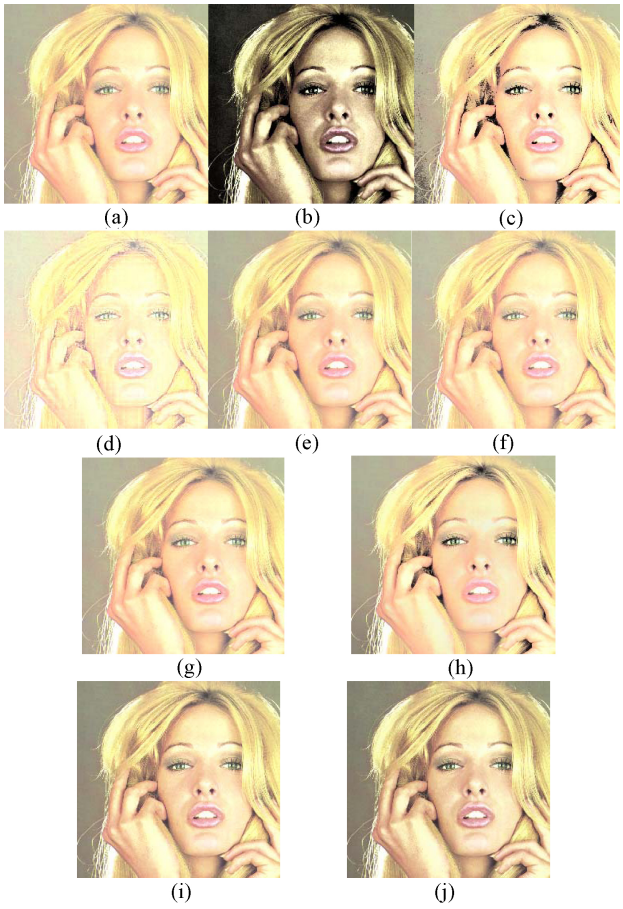

Fig. 17. Comparison of enhancement results. (a) Original image. (b) Histogram equalization. (c) Bi-histogram equalization method [4]. (d) TW-CES-BLK [23]. (e) DRC-CES-BLK [23]. (f) SF-CES-BLK [23]. (g) MSR [17]. (h) BSPICE. (i) S-BSPICE (early-stopping, four iterations). (j) S-BSPICE (six iterations, stopping criterion is satisfied).

TABLE X
COMPARISONS OF EXECUTION TIME FOR DIFFERENT ALGORITHMS (UNIT: SECONDS)

Image / Approach	Image in Fig. 15 (342 × 256)	Image in Fig. 16 (300 × 200)	Image in Fig. 17 (256 × 248)
HE	0.45	0.41	0.39
BHE	0.51	0.37	0.40
TW-CES-BLK	1.43	1.03	1.09
DRC-CES-BLK	1.77	1.07	1.01
SF-CES-BLK	1.43	1.21	1.04
BSPICE	1919.23	810.53	326.04
S-BSPICE (early stopping)	4.17 (three iterations)	2.77 (three iterations)	3.58 (four iterations)

IV. CONCLUSION

An efficient Bayesian framework for image enhancement was proposed in this paper. Unlike previous approaches, the proposed method considers the issues that may influence the visual quality of the captured image, including shutter speed and camera response function. Besides, statistical properties of nature images are also included in the algorithm for natural,

less-noise enhancement results. The benchmark image quality measures, including the discrete entropy, Brenner's measure and EME value, indicate the superiority of the proposed method. Moreover, to fit the requirement of practical applications, we further simplify the estimation process into an intensity mapping process. Simulation results of the simplified method verify the feasibility of the proposed algorithm in the task of image enhancement.

REFERENCES

[1] R. C. Gonzalez and R. E. Woods, *Digital Image Processing*. Reading, MA: Addison-Wesley, 2002.

[2] Y. T. Kim, "Contrast enhancement using brightness preserving bi-histogram equalization," *IEEE Trans. Consumer Electron.*, vol. 43, no. 1, pp. 1–8, Feb. 1997.

[3] Y. Wang, Q. Chen, and B. Zhang, "Image enhancement based on equal area qualistic subimage histogram equalization," *IEEE Trans. Consumer Electron.*, vol. 45, no. 1, pp. 68–75, Feb. 1999.

[4] S. Chen and A. R. Ramli, "Minimum mean brightness error bi-histogram equalization in contrast enhancement," *IEEE Trans. Consumer Electron.*, vol. 49, no. 4, pp. 1310–1319, Nov. 2003.

[5] S. Chen and R. Ramli, "Contrast enhancement using recursive mean-separate histogram equalization for scalable brightness preserving," *IEEE Trans. Consumer Electron.*, vol. 49, no. 4, pp. 1301–1309, Nov. 2003.

[6] H. Ibrahim, N. Sia, and P. Kong, "Brightness preserving dynamic histogram equalization for image contrast enhancement," *IEEE Trans. Consumer Electron.*, vol. 53, no. 4, pp. 1752–1758, Nov. 2007.

[7] M. Kim and M. G. Chung, "Recursively separated and weighed histogram equalization for brightness preservation and contrast enhancement," *IEEE Trans. Consumer Electron.*, vol. 54, no. 3, pp. 1389–1397, Aug. 2008.

[8] S. Yang, J. H. Oh, and Y. Park, "Contrast enhancement using histogram equalization with bin underflow and bin overflow," in *Proc. IEEE Int. Conf. Image Process.*, Sep. 2003, pp. 881–884.

[9] Q. Wang and R. K. Ward, "Fast image/video contrast enhancement based on weighed threshold histogram equalization," *IEEE Trans. Consumer Electron.*, vol. 53, no. 2, pp. 757–764, May 2007.

[10] T. Arici, S. Dikbas, and Y. Altunbasak, "A histogram modification framework and its application for image contrast enhancement," *IEEE Trans. Image Process.*, vol. 18, no. 9, pp. 1921–1935, Sep. 2009.

[11] J. A. Stark, "Adaptive image contrast enhancement using generalizations of histogram equalization," *IEEE Trans. Image Process.*, vol. 9, no. 5, pp. 889–896, May 2000.

[12] Z. Y. Chen, B. R. Abidi, D. L. Page, and M. A. Abidi, "Gray level grouping (GLG): An automatic method for optimized image contrast enhancement—-part 1: The basic method," *IEEE Trans. Image Process.*, vol. 15, no. 8, pp. 2290–2302, Aug. 2006.

[13] Z. Y. Chen, B. R. Abidi, D. L. Page, and M. A. Abidi, "Gray level grouping (GLG): An automatic method for optimized image contrast enhancement—-part 2: The variations," *IEEE Trans. Image Process.*, vol. 15, no. 8, pp. 2303–2314, Aug. 2006.

[14] T. K. Kim, J. K. Paik, and B. S. Kang, "Contrast enhancement system using spatially adaptive histogram equalization with temporal filtering," *IEEE Trans. Consumer Electron.*, vol. 44, no. 1, pp. 82–87, Feb. 1998.

[15] J. Y. Kim, L. S. Kim, and S. H. Hwang, "An advanced contrast enhancement using partially overlapped sub-block histogram equalization," *IEEE Trans. Circuits Syst. Video Technol.*, vol. 11, no. 4, pp. 475–484, Apr. 2001.

[16] D. J. Jobson, Z.-U. Rahman, and G. A. Woodell, "Properties and performance of a center/surround retinex," *IEEE Trans. Image Process.*, vol. 6, no. 3, pp. 451–462, Mar. 1997.

[17] D. J. Jobson, Z.-U. Rahman, and G. A. Woodell, "A multiscale retinex for bridging the gap between color images and the human observation of scenes," *IEEE Trans. Image Process.*, vol. 6, no. 7, pp. 965–976, Jul. 1997.

[18] R. Kimmel, M. Elad, D. Shaked, R. Keshet, and I. Sobel, "A variational framework for retinex," *Int. J. Comput. Vis.*, vol. 52, no. 1, pp. 7–23, 2003.

[19] L. Tao, R. Tompkins, and V. K. Asari, "An illuminance-reflectance model for nonlinear enhancement of color images," in *Proc. IEEE Comput. Soc. Conf. Comput. Vis. Pattern Recognit.*, Jun. 2005, pp. 159–166.

[20] S. Aghagolzadeh and O. K. Ersoy, "Transform image enhancement," *Opt. Eng.*, vol. 31, no. 3, p. 614, Mar. 1992.

[21] J. Tang, E. P. Peli, and S. Acton, "Image enhancement using a contrast measure in the compressed domain," *IEEE Signal Process. Lett.*, vol. 10, no. 10, pp. 289–292, Oct. 2003.

[22] S. Lee, "An efficient content-based image enhancement in the compressed domain using retinex theory," *IEEE Trans. Circuits Syst. Video Technol.*, vol. 17, no. 2, pp. 199–213, Feb. 2007.

[23] J. Mukherjee and S. K. Mitra, "Enhancement of color images by scaling the DCT coefficients," *IEEE Trans. Image Process.*, vol. 17, no. 10, pp. 1783–1794, Oct. 2008.

[24] C. Wang and Z. Ye, "Brightness preservation histogram equalization with maximum entropy: A variational perspective," *IEEE Trans. Consumer Electron.*, vol. 51, no. 4, pp. 1326–1334, Nov. 2005.

[25] I. Jafar and H. Ying, "Image contrast enhancement by constrained variational histogram equalization," in *Proc. IEEE EIT*, May 2007, pp. 120–125.

[26] M.-S. Shyu and J.-J. Leou, "A genetic algorithm approach to color image enhancement," *Pattern Recognit.*, vol. 31, no. 7, pp. 871–880, 1998.

[27] C. Munteanu and A. Rosa, "Gray-scale image enhancement as an automatic process driven by evolution," *IEEE Trans. Syst. Man Cybern. Part B Cybern.*, vol. 34, no. 2, pp. 1292–1298, Apr. 2004.

[28] Q. Shan, J. Jia, and M. S. Brown, "Globally optimized linear windowed tone-mapping," *IEEE Trans. Visualization Comput. Graph.*, vol. 16, no. 4, pp. 663–675, Jul.–Aug. 2010.

[29] T. C. Jen and S. J. Wang, "An efficient Bayesian framework for image enhancement with spatial consideration," in *Proc. IEEE Int. Conf. Image Process.*, Sep. 2010, pp. 3285–3288.

[30] P. E. Debeve and J. Malik, "Recovering high dynamic range radiance maps from photographs," in *Proc. ACM SIGGRAPH*, Aug. 1997, pp. 369–378.

[31] S. Roth and M. J. Black, "Field of experts: A framework for learning image priors," in *Proc. IEEE Int. Conf. Comput. Vis. Pattern Recognition*, Jun. 2005, pp. 860–867.

[32] E. K. P. Chong and S. H. Zak, *An Introduction to Optimization*. New York: Wiley, 2001.

[33] S. Boyd and L. Vandenberghe, *Convex Optimization*. Cambridge, U.K.: Cambridge University Press, 2004.

[34] M. Schmidt, E. van den Berg, M. Friedlander, and K. Murphy, "Optimizing costly functions with simple constraints: A limited-memory projected quasi-Newton algorithm," in *Proc. 12th Int. Conf. Artif. Intell. Statist.*, Apr. 2009, pp. 456–463.

[35] S. S. Agaian, B. Silver, and K. A. Panetta, "Transform coefficient histogram-based image enhancement algorithms using contrast entropy," *IEEE Trans. Image Process.*, vol. 16, no. 3, pp. 741–758, Mar. 2007.

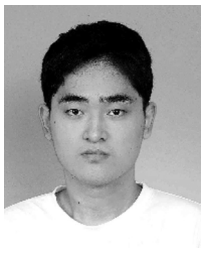

Tzu-Cheng Jen received the B.S. degree in electrical and control engineering and the M.S. degree in electronics engineering, both from National Chiao Tung University, Hsinchu, Taiwan, in 2002 and 2004, respectively. He is currently pursuing the Ph.D. degree in electronics engineering with the Department of Electronics Engineering, Institute of Electronic, National Chiao Tung University.

His current research interests include image/video processing and computer vision.

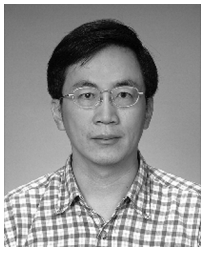

Sheng-Jyh Wang (M'95) received the B.S. degree in electronics engineering from National Chiao Tung University (NCTU), Hsinchu, Taiwan, in 1984, and the M.S. and Ph.D. degrees in electrical engineering from Stanford University, Stanford, CA, in 1990 and 1995, respectively.

He is currently a Professor with the Department of Electronics Engineering, Institute of Electronic, NCTU. His current research interests include image processing, video processing, and image analysis.